Morphology and Optical Property Changes of Nanostructured Tungsten in LHD

Shin KAJITA, Tsuyoshi AKIYAMA[1)], Naoaki YOSHIDA[2)], Masayuki TOKITANI[1)], Miyuki YAJIMA[1)] and Noriyasu OHNO[3)]

EcoTopia Science Institute, Nagoya University, Nagoya 464-8603, Japan
[1)]*National Institute for Fusion Science, Toki 509-5292, Japan*
[2)]*Research Institute for Applied Mechanics, Kyushu University, Kasuga, Fukuoka 816-8580, Japan*
[3)]*Graduate School of Engineering, Nagoya University, Nagoya 464-8603, Japan*

(Received 21 May 2015 / Accepted 16 September 2015)

Nanostructured tungsten formed by the exposure to helium plasma in a linear plasma device was installed in the large helical device (LHD). After the exposure in a series of experiments in the 2012 fiscal year campaign in LHD, the samples were analyzed by scanning electron microscope (SEM), transmission electron microscope (TEM), and energy dispersion x-ray spectroscopy (EDX). It was found that part of the nanostructures was totally covered with carbon based material probably from divertor, while some other parts were eroded by sputtering. On the erosion dominant region, it was revealed that the head part of nanostructures was sputtered and the surface became rounded, but the nanostructures still remained near the surface. Optical reflectance of the material was measured, and it was found that the morphology changes increased the optical reflectivity up to ∼10% from typically less than 1%. The possibility and limitation of the nanostructured tungsten as a light absorber (viewing dump) are discussed.

Keywords: nanostructured tungsten, large helical device (LHD), deposition, sputtering

DOI: 10.1585/pfr.10.1402083

1. Introduction

In fusion devices, tungsten (W) is one of the most plausible materials for plasma facing components including first wall and divertor tiles, because of its high durability for erosion by plasma bombardment and low tritium retention property. One of the issues arising from the usage of W is an influence of reflection of light on optical diagnostics, so-called stray light problem. Because the optical reflectance of W is much higher than that of carbon based materials, the influence of light reflection on the wall becomes much severer in full W devices. Especially, since line emissions from divertor region can be much higher than those in the scrape off layer (SOL) region, the emission from the SOL are to be perturbed significantly.

The stray light issue has been discussed even in present devices such as DIII-D [1], Alcator C-Mod [2], and Tore-supra [3, 4]. Recent stray light modeling study of H_α monitor system of SOL region in ITER indicated that the stray light level in ITER will be several orders of magnitude greater than the actual signal [5]. Moreover, it was found that the influence of stray light would not be negligible also in divertor region [6]. Even for charge exchange recombination spectroscopy, theoretical modeling demonstrated that the stray light issue can be serious in ITER, because the beam attenuation is much greater than that in the present devices due to high density and the large device size [7].

One of the ways to mitigate the stray light problem is a usage of an optical viewing dump with dark material. From plasma material interaction researches, it has been found that the irradiation of helium (He) particles to W leads to nanostructure formation [8]; it has been revealed that the material is the darkest man made metal and can be used for light absorber from ultra-violet and near infrared wavelength range [9]. It is of interest to investigate whether it could be used for the material of viewing dump. The advantages are that the nanostructure is composed of pure W and the surface morphology can be controlled by plasma irradiation. However, it has yet to be reported how morphology and optical property of the nanostructured material altered during the exposure in fusion devices. It is of importance to investigate how the processes of sputtering, deposition, and so on change the surface morphology and optical property.

In this study, the nanostructured W samples are fabricated in the linear plasma device NAGDIS (Nagoya Divertor Simulator)-II and installed in the large helical device (LHD), and the morphology changes by the exposure in LHD are investigated. There were several studies investigating the changes of nanostructures by the exposure to divertor plasmas in tokamak or helical devices [10, 11].

author's e-mail: kajita.shin@nagoya-u.jp

It has been reported that nanostructures were eroded and an arcing was initiated by the exposure to the high density plasmas. Different from those studies, the present paper investigates the morphology changes during the exposure to neutral particles, i.e., charge exchange (CX) and sputtered neutral particles, in vacuum vessel. The surface morphology changes are analyzed in detail using scanning electron microscope (SEM) and transmission electron microscope (TEM), and, moreover, the optical property and the chemical composition of the surface are characterized. Degradation of optical absorptance and the influences of CX particles and deposition on the surface are revealed.

2. Setup

W samples (Nilaco. co.) were exposed to the helium (He) plasma in NAGDIS-II [8] to fabricate nanostructures on the surface. The thickness of the sample was 0.2 mm. Figures 1 (a) and (b) show pictures of the samples equipped on the LHD vacuum vessel. The position was not far from the divertor tiles, which was composed of isotropic graphite. Four samples with the size of 30×30 mm were installed in array. The samples were electrically isolated from the vacuum vessel (VV), which was grounded. One sample was separately installed and electrically connected to VV to see the difference. The samples were named W1-W5, as shown in Fig. 1 (b). The irradiation with the He plasma in NAGDIS-II was conducted at the surface temperature of 1200 K and the incident ion energy of ~50 eV for W1-W5. The irradiated He fluence was 1.0×10^{26} m^{-2}.

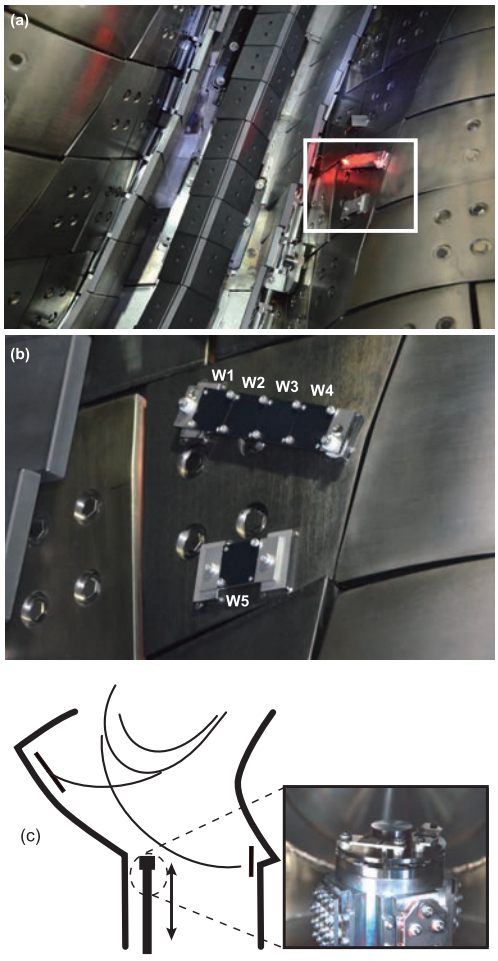

Fig. 1 (a, b) Pictures of the samples equipped in the LHD vacuum vessel and (c) a schematic of the configuration of the sample holder in LHD.

The samples were exposed in all the series of experiments in fiscal year 2012 (2012FY) campaign of LHD including glow and main discharges. In the 2012FY campaign in LHD, 5000 hydrogen discharges and 300 helium discharges were conducted. Concerning the glow discharge, He, hydrogen (H), and neon (Ne) gases were used for discharge. Totally, the durations of He, H, and Ne glow discharges were 48, 24, and 6 hours, respectively.

In addition to the samples mounted on the vacuum vessel, movable sample holder was used to see the influence in distinct exposure times. Figure 1 (c) shows a schematic of the configuration of the sample holder. Two samples with the size of 10×10 mm can be mounted on the holder: one is electrically connected to and the other is electrically isolated from the vacuum vessel. Two samples (W6-W7) were installed during the LHD glow discharge phase and another two samples (W8-W9) were installed during the main discharges. Since they were installed using the movable sample holder, they can be exchanged within the experimental campaign. The irradiation of the He plasma was conducted at the surface temperature of 1300 K and the incident ion energy of ~50 eV. The irradiated He fluence for W6-W9 was 1.0×10^{26} m^{-2}, which was the same as that of W1-W5. It is noted that the position of the sample holder can be changed. During the glow discharge, the sample holder was lowered approximately 1.5 m from the VV, while in the main discharge the level of the sample holder was same as that of the VV.

After the exposure in LHD, the absolute optical reflectance of the sample was measured using a helium neon laser at the wavelength of 633 nm and an integrating sphere equipped with a photodetector [9]. The sample was mounted in the center of the integrating sphere and the intensity of the light redistributed in the integrating sphere was measured with the photodetector. The incident angle of the laser was almost normal to the sample. Typical reflectance of the sample before installation was 0.47% for the sample with the size of 10×10 mm irradiated at 1300 K. Previously, the reflectance of the sample with the fluence of ~ 5×10^{25} m^{-2} was measured to be 0.7% [9]. It is likely that an increase in the He fluence decreased the reflectance further.

3. Results

3.1 Exposure in whole 2012FY campaign

Figures 2 (a)-(c) show SEM micrographs of W1, W3, and W5, respectively. On W1, though structures be-

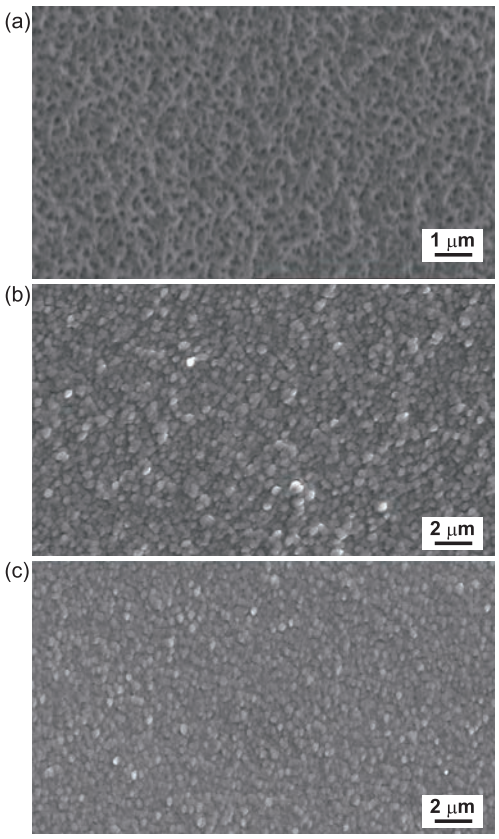

Fig. 2 SEM micrographs of (a) W1, (b) W3, and (c) W5 after the exposure in LHD.

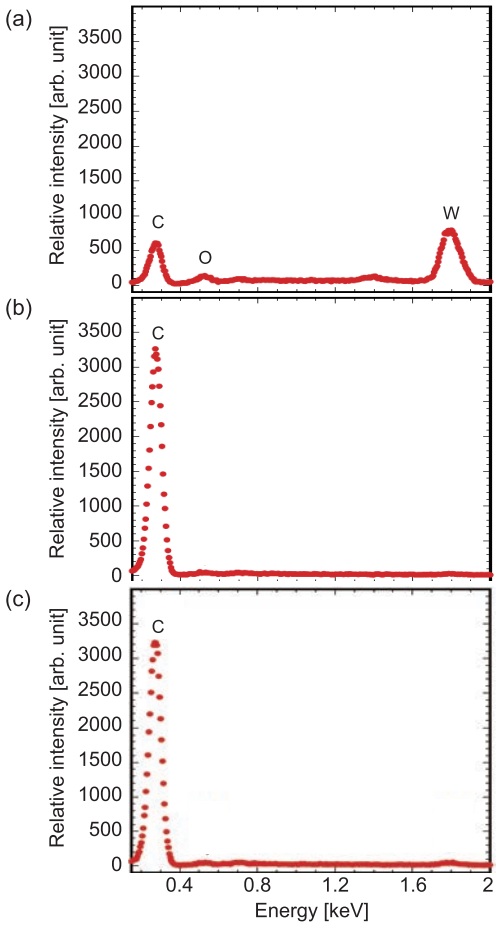

Fig. 3 EDX spectra of (a) W1, (b) W3, and (c) W5.

Table 1 The conditions of the samples exposed in LHD and optical reflectance measured after the exposure was summarized.

Sample	location	potential	Reflectance [%]
W1	VV	floating	6.3
W2	VV	floating	–
W3	VV	floating	–
W4	VV	floating	10.3
W5	VV	ground	9.9
W6	stage	ground	3.7
W7	stage	floating	1.3
W8	stage	ground	1.7
W9	stage	floating	1.1

came rounded, pinholes can be identified and fine structure seems to still remain partially. On the other hand, on W3 and W5, fine nanostructures disappeared from the surface totally. The optical reflectance of the sample was changed by the exposure to the particles from the plasma. In Table 1, the condition of exposure and the optical reflectance of the samples measured after the exposure were shown. For the samples W4-5, the reflectance was ~10% or more. The reflectance of W1 was less than that of W4-5, but it was increased by the exposure significantly. The measurements were conducted only on the both ends of the samples, i.e., W1 and W4. It is likely that the reflectance of W2 and W3 is in between that of W1 and W4, i.e. in the range of 6 - 10%.

Figures 3 (a)-(c) show the energy dispersion x-ray spectroscopy (EDX) spectra of W1, W3, and W5, respectively. In Fig. 3 (a), three distinct peaks can be identified on the EDX spectra, corresponding to characteristic x-ray energies of 0.277 keV for carbon (C), 0.525 KeV for oxygen (O), and 1.775 keV for W. Only the carbon peak was identified on W3 and W5, indicating that the W nanostructures were totally covered by carbon deposition. It was confirmed that the surface of W3 and W5 seen Figs. 2 (b) and (c) are the deposited carbon from divertor. On the other hand, on W1, W peak can be identified as well as carbon and oxygen. On W1, because a shadow from the divertor tiles was formed by a baffle plate, carbon deposition was less than the other samples. For the oxygen peak, probably part of W was oxidized after the exposure to the air before the EDX analysis.

It has been observed that nanostructures were reintegrated to the surface when they were heated up to typically > 1200 K without He plasma irradiation [12, 13]. By

the thermal treatment, the nanostructures disappeared from the surface and flat surface was recovered. The surface of W1 was different from the one with the thermal treatment. To investigate the sample in detail, a thin (~100 nm) cross sectional sample was prepared by focused ion beam (FIB) technique and analyzed by TEM.

Figures 4 (a)-(c) show TEM micrographs of the cross section of W1. It is seen that nanostructures still exist on the surface. The thickness of the nanostructured layer was approximately 350 nm. Usually, on the grown nanostructures by He plasma irradiation, the head part of the structures was directed in various directions [9]. However, after the exposure in LHD, the top part was crushed and rounded. It is likely that this structural change and C deposition shown in Fig. 3 (a) leads to the recovery of the optical reflectance to ~6%.

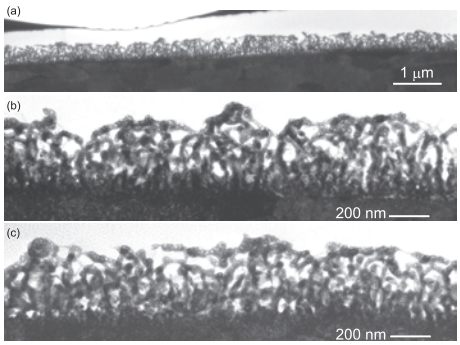

Fig. 4 TEM micrographs of the cross section of W1. (a) and (b, c) are in different magnifications and (b) and (c) show different position in the same magnification.

Figures 5 (a) and (b) show TEM micrographs in a larger scale. Inside the structures closer to the surface, large amount of He bubbles are formed. Considering the fact that the number of bubbles is so significant, it is likely that He glow discharge cleaning and He main discharge have contributed to form new He bubbles near the surface. Since the surface temperature was much lower during the exposure in LHD, the newly formed bubbles should have much smaller sizes than those initially formed. Figures 5 (c) and (d) show TEM micrographs of the head part and bottom part of the structures, respectively, in a larger magnification. In particular, the head part exhibits a distinct morphology change by the exposure. In some parts, bubbles appeared on the fiber surfaces, as shown with red arrows in Fig. 5 (c). Nanostructures were damaged by the sputtering and the surface of fibers became much rougher. Recently, detailed analysis of TEM observation of the nanostructures were conducted from various points of view including its multi-fractal features [14]. It was found that the width (diameter) of the nanostructures formed by the irradiation at ~1400 K has a distribution in the range of 10 - 30 nm and that the nano-fibers frequently had narrow parts, which was probably formed by the bursting of bubbles from the side of the fiber. However, any fiber with bubbles on the fiber surface has never been seen. Even if bubbles reached on the surface during the irradiation, the hollow structures should be smoothed out since the temperature was much higher. During the exposure in LHD, since the surface temperature should be much lower than 1000 K, the roughness of bubbles remained even af-

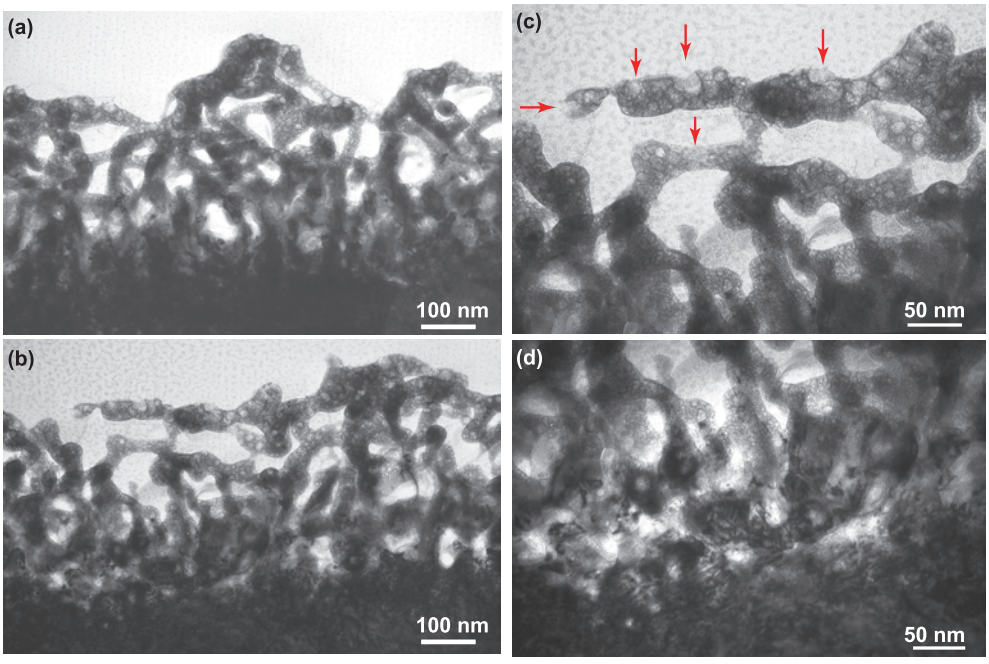

Fig. 5 TEM micrographs of the cross section of W1. (a) and (b) are from the same sample but at different positions. (c) and (d) show the head part and bottom part of the structures, respectively, in a larger magnification.

ter the fibers were sputtered and bubbles reached the surface. Because the roughness of fibers should be enhanced by the sputtering process, the effective surface area could be increased. On the other hand, for the bottom part of the structure, number of small bubbles is much less than that in the head part. It seems that newly formed bubbles are negligible in this region.

3.2 Exposure in glow discharges

Figures 6 (a) and (b) show SEM micrographs of W6, which was exposed to glow discharges (neon discharge for 3 h and H discharge for 24 h) at the ground potential, observed from top (0 degree) and 60 degree, respectively. Despite the fact that the sample was far (~1.5 m) from the deposition source, the surface was covered by deposition, and the nanostructures were not observed on the surface. From Fig. 6 (b), which is observed from an oblique direction, the surface roughness can be clearly identified.

Figures 7 (a)-(c) show TEM micrographs of W6 in different magnifications. The sample was fabricated by FIB, and the thickness of the sample was ~300 nm. It was found that the beneath the covered top layer, fine nanostructures with the thickness of ~ 1 μm existed without any significant damages by sputtering. No clear deposition was identified around the nanostructures in the TEM micrograph, probably because the transmission of electrons on the deposition layer is much higher than W. It is likely that deposition should have occurred on W6, as seen in the SEM micrograph in Fig. 6.

Figures 8 (a) and (b) show SEM micrographs of W7 observed from top (0 degree) and 60 degree, respectively. The sample was exposed to the glow discharges at the floating potential. The nanostructures were also disappeared from the surface; the surface roughness was different from W6. The surface of W6 was rough and the structure has sharp edges in some parts. On the other hands, the surface of W7 has finer round shaped structures on the surface. The measured optical reflectances of W6 and W7 were 3.7

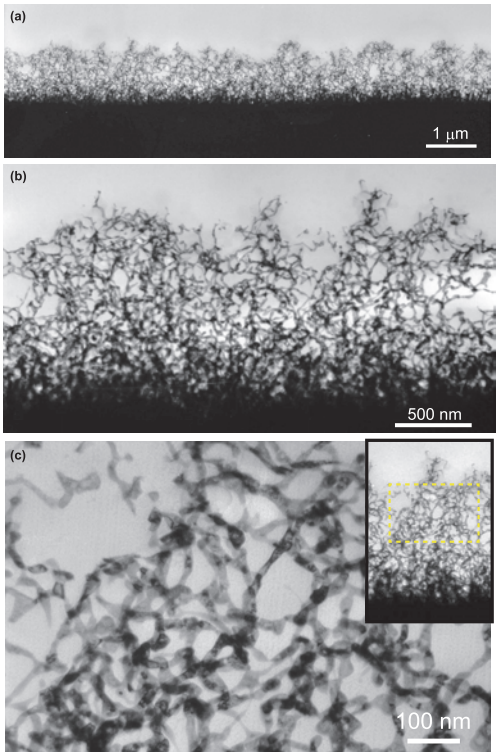

Fig. 7 TEM micrographs of W6 in different scales.

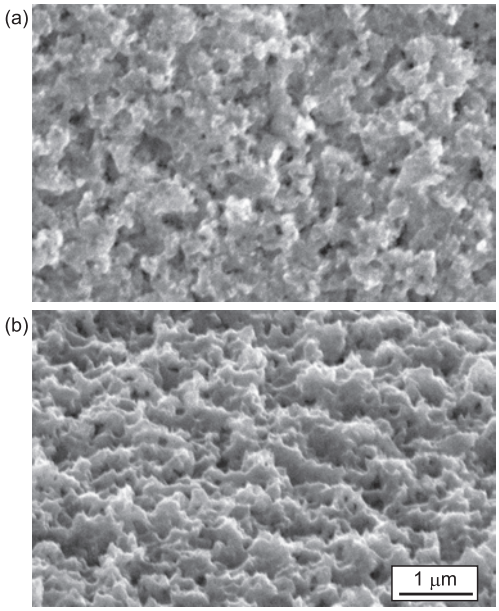

Fig. 6 SEM micrographs of W6 observed (a) from top (0 degree) and (b) from obliquely (60 degree).

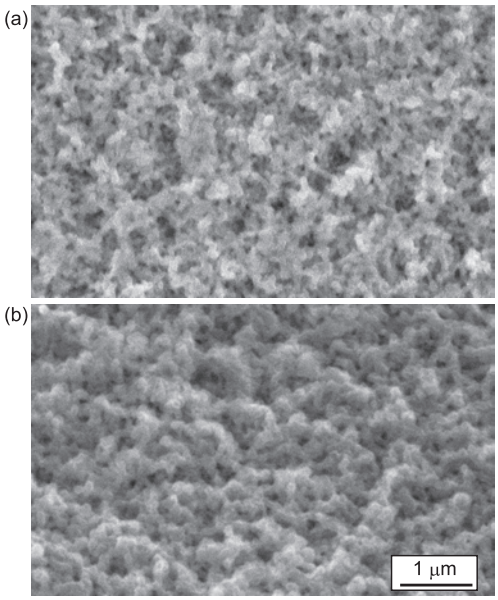

Fig. 8 SEM micrographs of W7 observed (a) from top (0 degree) and (b) from 60 degree.

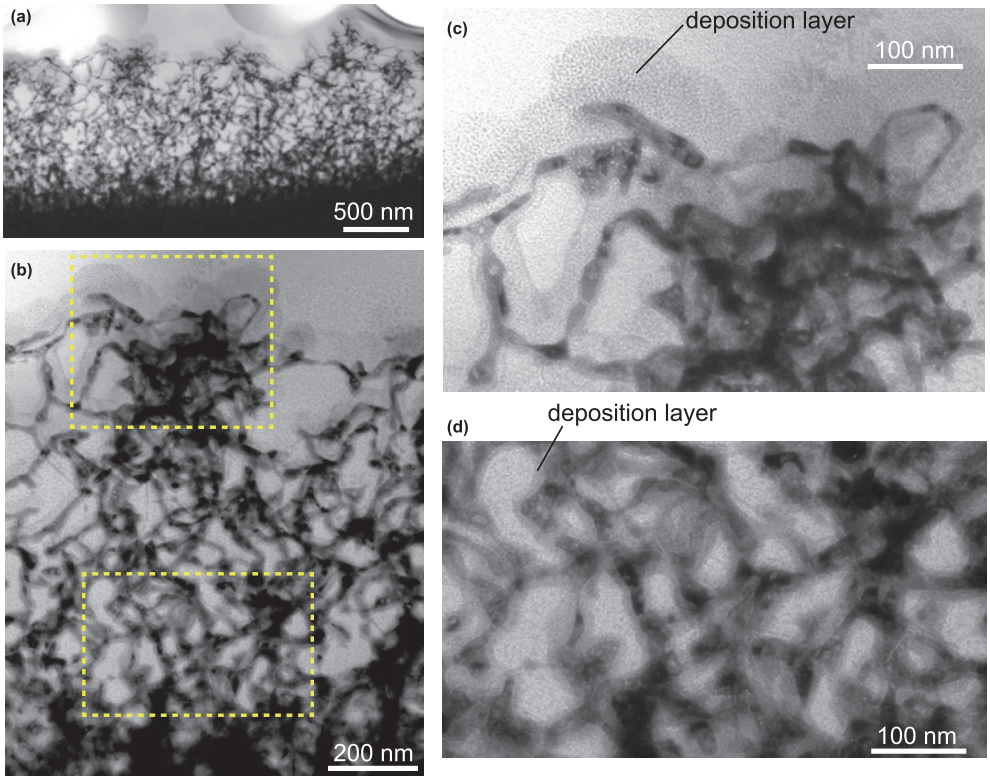

Fig. 9 TEM micrographs of W7 in different scales. (c) and (d) are the top part and deep part of the structures.

and 1.3%, respectively. The nanostructured surface and bulk surface should have the lowest and highest optical reflectance, respectively. From the SEM analysis, it was seen that the original nanostructure still remained on W7 surface even with deposition, while the traces of original surface disappeared from W6. We thought that difference of the optical reflectance can be attributed to the surface morphology.

Figure 9 shows TEM micrograph of the sample W7. It was found that the nanostructures are fully remained even on W7. On the top of the nanostructure, shown in Fig. 9 (c), however, deposition layer with the thickness over 70 nm is observed. In deeper region shown in Fig. 9 (c), deposition was also identified with the thickness >10 nm.

During Ne glow discharges, it is likely that sputtering occurred on the surface of W6. However, the width of W nanostructures on W6 did not change from that on W7 without considering the deposition layers, indicating that the trace of sputtering was not identified from the TEM micrographs. This is because the position of the stage was 1.5 m far from VV and the ion flux was significantly lower than that when the position of stage was at the same level of VV. From SEM micrographs shown in Figs. 6 and 8, the surface of W7 has finer structures, though both of the samples likely to have depositions. During glow discharges, the incident ion energy is ~500 eV for the sample at the ground potential (W6), while it is much lower, say several times the electron temperature, for the sample at the floating potential (W7). Physical sputtering operates only on

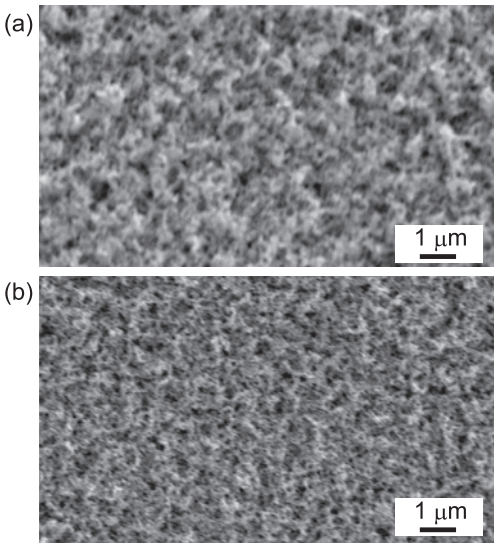

Fig. 10 SEM micrographs of (a) W8 and (b) W9.

W6; difference between W6 and W7 was probably caused by the physical sputtering occurred on the deposition layer on W6. It is known that surface becomes smooth when physical sputtering operates on surface [15].

3.3 Exposure in main discharges

Figures 10 (a) and (b) are SEM micrographs of W8 and W9, respectively, which were exposed to long pulse discharges in LHD for two days using the movable sample

holder at the floating potential (W8) and ground potential (W9). The position of the samples is the same level as the VV. The samples were exposed to ICH and ECH heating discharges for 1000 s on the first day and ECH heating discharges for 1000 s on the second day. Even after the long pulse discharges, the nanostructures still remained on the surface. The optical reflectance was slightly increased and was 1.7% on W8 and 1.1% on W9. In the analogy to the difference in the optical reflectance between W1 and W4, the slight difference of the reflectance between W8 and W9 can be caused by the difference in the location, since the particle flux on the surface may alter by location. Since the color of the head part of the sample holder was darkened after the exposure, it is likely that carbon deposition mainly occurred during the time period and the deposition changed the optical reflectance. In main discharges, the particles reaching the surface were mainly neutrals. Thus, it is understandable that no clear differences appeared on the morphology changes and reflectances.

4. Discussion

It was found from the SEM analysis that deposition occurred on W2-W5 and W6-7. Moreover, erosion by sputtering and additional He bubble formation were identified on W1. To use nanostructures for the viewing dump practically, the results indicated that it is necessary to decrease the influence of the deposition and sputtering. The same should be true even for the other materials with special textures in sub-micron scale to reduce the optical reflectance. One method is of course to manufacture a viewing dump without using such fine textured materials; however, they are still attractive because it can decrease the stray light level further [5].

In long pulse discharges in LHD, the deposition amount was measured recently [16]. It was revealed that the thickness of the deposition layer increases with the exposure time almost proportionally at the deposition rate of $\sim$1/200 nms^{-1}. On the samples W8 and W9, which were exposed to the LHD long pulse discharges for 2000 s, it is likely that carbon deposition with a thickness of $\sim$ 10 nm occurred. It is thought that the width of nanostructure increased by the deposition, and consequently, the optical reflectance increased, although the changes in that scale could not be identified by SEM analysis. Considering the fact that the width of the nanostructures is several tens of nanometers, deposition exceeding 100 nm would totally kill the advantage of the nanostructures as a optical absorber, such as W4-5. Moreover, as seen on W6 and W7, it is likely that the deposition during glow discharges are also considerable as well as the main discharges.

It is likely that the deposition is unavoidable, because neutral particles can fly far from the plasma. Thus, first, it can be said that a mechanical shutter is inevitable to mitigate those influences. It is necessary to close the shutter during glow discharge cleaning and times when the measurement was not conducted. Also, from the fact that the deposition on W1 was less than the others, it can be said that particles deposited on the surface has directionality, i.e. from divertor tile in the present case, especially in main discharges. A shielding wall or material to reduce deposition by directional particle flows would also be effective.

It was estimated from the analysis of plasma facing wall in LHD that the averaged CX particle flux and energy at the first wall in LHD were $\sim 10^{19}$ m^{2}s^{-1} and 1 - 2 keV during main discharges [17]. In the 2012FY campaign, 5000 H discharges and 300 He discharges were performed. Typical duration of the high density short time discharge was approximately 2 s. Roughly, the estimated He and H fluences during the main discharges are 0.6×10^{22} and 1×10^{23} m^{-2}, respectively. There were long pulse discharges in addition to the short pulse discharges. The particle flux in the long pulse discharge is approximately one order of magnitude lower than short pulse discharges, though the average discharge duration can be several fold if we include the long pulse discharges. We should say that the actual fluences can be higher than the estimated fluences.

In main discharge, since the energy of CX particles is 1 - 2 keV, the energy is high enough to form lattice defects by the bombardment to W. From the TEM micrographs of the top part of the sample W1, it was identified that additional small He bubbles were formed during the exposure. The He fluence of 1×10^{22} m^{-2} is sufficient to form He bubbles [18]. However, the fluence and the temperature were not sufficient to grow nanostructures; bubble formation only proceeded without changing the structure shape.

During the glow discharges, the particle flux and the energy are $\sim 10^{17}$ m^{-2} and $\sim$500 eV, respectively. The total times of glow discharge in 2012FY campaign are 6 h for Ne, 48 h for He, and 24 h for H. The particle fluences are estimated to be 2.2×10^{21} m^{-2} for Ne, 1.7×10^{22} m^{-2} for He, and 8.6×10^{22} m^{-2} for H during the glow discharge cleaning.

In Table 2, estimated fluence and erosion depth of W in glow and main discharges by each species are summarized. Here, the erosion depth was estimated from the sputtering yield and particle fluence [19]. From the estimated

Table 2 Estimated fluence and erosion depth in glow and main discharges in FY2012 campaign.

Species	Discharge	Energy [keV]	Fluence [m^{-2}]	Erosion [nm]
H	glow	0.5	8.6×10^{22}	0.2
He	glow	0.5	1.7×10^{22}	5.5
Ne	glow	0.5	2.2×10^{21}	11
H	main	2.0	1×10^{23}	3.9
He	main	2.0	0.6×10^{22}	5

particle fluences, it is likely that the main contribution is from Ne and He glow discharges and He and H main discharges. It is noted that the potential of W1 was at the floating potential; the glow discharge did not work for erosion. The summation of the value in Table 2 corresponds to the estimated erosion depth. It is estimated that the erosion depths during the glow and main discharges are 16.7 and 8.9 nm, respectively, and total erosion depth is ~25 nm, which is comparable to the width of nanostructures. However, from the SEM and TEM micrographs of W1, it was seen that the surface morphology was changed significantly by erosion, indicating the possibility that the actual erosion is much more than the estimated erosion depth of 25 nm. In Table 2, influence of long pulse discharges were omitted; it can increase the erosion, but it is unlikely that the contribution increased the amount significantly. Even though the total time of long pulse discharges was several times that of the short pulse discharges, because the flux was one order of magnitude lower in the long pulse discharge, the total particle flux would not exceed twice the estimated value.

Recently, it was demonstrated that the erosion rate of the top of nanostructures is consistent with the erosion rate obtained by the conventional sputtering yield [20]. In [20], the irradiation direction was always normal. Since the CX particles impinge on the surface from various directions, the sputtering yield might be increased in the present case. For ex., the sputtering yield of W by He at 2 keV is four times greater than that at the normal direction when the incident angle is 75 degree [19]. Concerning the erosion of nanostructures by particles bombarded obliquely, further investigation with some special experiments will be of importance for future work.

5. Summary

Blackened nanostructured tungsten samples prepared by the exposure to a helium plasma in the linear plasma device NAGDIS-II were installed to LHD, and the variation in morphology changes and optical reflectance after the exposure were investigated in detail.

On the samples exposed to glow discharges (neon discharge for 3 h and H discharge for 24 h), significant depositions occurred on the samples when the sample was at the floating potential even though the samples were far (~1.5 m) from the vacuum vessel. Deposition layer with the typical thickness of 10 - 70 nm was formed on the nanostructures. When the sample was grounded, surface was flattened by the physical sputtering of the deposited layer and reflectance became 3.7% from the typical reflectance of the sample of 0.5%, while the reflectance was 1.3% for the sample exposed at the floating potential. On the samples exposed to main discharges (long pulse discharges of 2000 s in total), the sample reflectance slightly increased, probably because of the combination of the deposition and sputtering.

For the samples exposed to the whole 2012FY campaign of LHD, almost all the samples except one were covered with carbon based deposition and nanostructures were not identified because of thick deposition on the surface. On one sample which was located close to a baffle plate, it was found from energy dispersion x-ray spectroscopy that tungsten was identified and nanostructures remained on the surface. It was likely that the baffle shielded carbon flow from the divertor. From the TEM micrograph analysis, erosion by sputtering occurs on the top part of nanostructures.

The usage of nanostructured material for viewing damp has an advantage that it can decrease significantly the extinction ratio of stray light, which may pose serious issue for optical diagnostics in full metallic devices. However, from this study, it was revealed that the absorptive property of nanostructures is deteriorated by the deposition and erosion by sputtering significantly. In ITER, deposition of beryllium is likely to occur. Thus, it is inevitable to seek a way to avert the deposition on the surface if we would use nanostructured materials for viewing dump. Considering the erosion by sputtering, moreover, it would be necessary to replace the nanostructured material regularly. To mitigate the deposition, it is necessary to equip a mechanical shutter. It would be beneficial for decreasing the influence of erosion by sputtering as well. A side cover that shields the deposition by directional particle flow would also be effective to mitigate the deposition.

Acknowledgements

We thank Mr. J. Kato graduated from Nagoya Univ. to support some experiments presented in this study. This work was supported in part by a Grant-in-Aid for Scientific Research (B) 15H04229 from the Japan Society for the Promotion of Science (JSPS) and NIFS collaborative research program (NIFS11KUHR013 and NIFS15KOAH032).

[1] E.M. Hollmann, A.Y. Pigarov and R.P. Doerner, Rev. Sci. Instrum. **74**, 3984 (2003).
[2] E.M. Hollmann and A.Y. Pigarov, Contrib. Plasma Phys. **44**, 301 (2004).
[3] R. Reichle, J.-P. Lasserre, F. Oelhoffen, C. Desgranges, F. Faisse, L. Eupherte, C. Pocheau and M. Todeschini, Physica Scripta **2009**, 014029 (2009).
[4] P. Lotte, M.H. Aumeunier, P. Devynck, C. Fenzi, V. Martin and J.M. Travere, Rev. Sci. Instrum. **81**, 10E120 (2010).
[5] S. Kajita, E. Veshchev, S. Lisgo, R. Reichle, R. Barnsley, M. Walsh, A. Alekseev, A. Gorshkov, D. Vukolov, J. Stuber and S. Woodruff, Plasma Phys. Control. Fusion **55**, 085020 (2013).
[6] S. Kajita, E. Veshchev, S. Lisgo, R. Barnsley, P. Morgan, M. Walsh, H. Ogawa, T. Sugie and K. Itami, J. Nucl. Mater. **463**, 936 (2015).
[7] S. Banerjee, P. Vasu, M. von Hellermann and R.J.E. Jaspers, Plasma Phys. Control. Fusion **52**, 125006 (2010).
[8] S. Takamura, N. Ohno, D. Nishijima and S. Kajita, Plasma Fusion Res. **1**, 051 (2006).
[9] S. Kajita, T. Saeki, N. Yoshida, N. Ohno and A. Iwamae,

Appl. Phys. Express **3**, 085204 (2010).
[10] Y. Ueda *et al.*, J. Nucl. Mater. **415**, S92 (2011).
[11] M. Tokitani, S. Kajita, S. Masuzaki, Y. Hirahata, N. Ohno, T. Tanabe and LHD Experiment Group, Nucl. Fusion **51**, 102001 (2011).
[12] M. Baldwin and R. Doerner, J. Nucl. Mater. **404**, 165 (2010).
[13] M. Yajima, N. Yoshida, S. Kajita, M. Tokitani, T. Baba and N. Ohno, J. Nucl. Mater. **449**, 9 (2014).
[14] S. Kajita, N. Yoshida, N. Ohno and Y. Tsuji, New J. Phys. **17**, 043038 (2015).
[15] L. Vazquez and J.G. Buijnsters, J. Appl. Phys. **106**, 033504 (2009).
[16] M. Tokitani, H. Kasahara, S. Masuzaki, G. Motojima, M. Shoji, Y. Ueda, N. Yoshida, Y. Yoshimura, K. Nagasaki, N. Ashikawa, T. Mutoh, H. Yamada and S. Nagata, J. Nucl. Mater. **463**, 91 (2015).
[17] M. Tokitani *et al.*, J. Nucl. Mater. **386-388**, 173 (2009).
[18] H. Iwakiri, K. Yasunaga, K. Morishita and N. Yoshida, J. Nucl. Mater. **283-287**, 1134 (2000).
[19] W. Eckstein, *Calculated Sputtering, Reflection and Range ValuesBericht / 9: Bericht* (IPP, 2002).
[20] Y. Noiri, S. Kajita and N. Ohno, J. Nucl. Mater. **463**, 285 (2015).